IEEE/CSC & ESAS European Superconductivity News Forum (ESNF), No. 6, October 2008
(ASC Preprint 5MA02 conforming to IEEE Policy on Electronic Dissemination, Section 8.1.9)
The published version of this manuscript appeared in *IEEE Transactions on Applied Superconductivity* **19**, No. 3, Part 3, 3451 - 3454 (2009)

YBCO Superconductors on Electrodeposited Biaxially Textured Buffer Layers

Raghu Bhattacharya, Sovannary Phok, Wenjun Zhao, and Andrew Norman

***Abstract*—Non-vacuum electrodeposition (ED) was used to prepare simplified $Gd_2O_3/Gd_2Zr_2O_7$ and $CeO_2/Gd_2Zr_2O_7$ buffer layers on a Ni-W substrate. Post-annealing conditions of electrodeposited precursor films were optimized to obtain high-quality biaxially textured buffer layers. The buffer layers were characterized by X-ray diffraction, optical profiling, and transmission electron microscopy. The effect of the cap layer thickness on the surface morphology and texture of the buffers was also studied. The microstructure of $CeO_2/Gd_2Zr_2O_7$ was analyzed and compared to $Gd_2O_3/Gd_2Zr_2O_7$. $YBa_2Cu_3O_{7-\delta}$ (YBCO) superconductor was deposited by pulsed laser deposition (PLD) on the simplified ED-$Gd_2O_3/Gd_2Zr_2O_7$ and ED-$CeO_2/Gd_2Zr_2O_7$ buffers. Transport current density of 3.3 MA/cm^2 was obtained for PLD YBCO deposited on ED-$Gd_2O_3/Gd_2Zr_2O_7$ buffer layers.**

***Index Terms*— Biaxial texture, buffer layers, electrodeposition, pulsed laser deposition, YBCO.**

I. INTRODUCTION

SUITABLE templates (substrate and buffer layers) are critical for the production of high-quality coated conductors. For the commercialization of high-quality superconductor wires, numerous factors related to the substrate, the buffer layers, and the YBCO superconductor need to be addressed. Among potential substrates, metallic substrates are particularly attractive based on their flexibility and availability in long lengths. High-temperature superconductors have shown great promise for practical applications. This is particularly true for YBCO fabricated on Ni-based alloys using the rolling-assisted biaxially textured substrate (RABiTS) technique [1], because of its minimal magnetic hysteresis loss, thermal and mechanical properties, and high-quality biaxial cube texturing [2]. Buffer layers as a chemical barrier, with suitable orientation and lattice match to form textured template, are required for such substrates for subsequent growth of epitaxial YBCO superconductor. Ceramic buffers offer excellent lattice match and high resistance to oxidation. High current densities (greater than MA/cm^2) in YBCO have been demonstrated on oxide buffers such as CeO_2 [3] and Gd_2O_3 [2].

At NREL, we are developing the simplified buffer layers by a non-vacuum electrodeposition process, which is potentially a low-cost technique [4]. In this paper, we are reporting on the electrodeposited $Gd_2O_3/Gd_2Zr_2O_7$ and $CeO_2/Gd_2Zr_2O_7$ buffer layers for subsequent growth of YBCO superconductors. The buffer layer was qualified by subsequent deposition of pulsed-laser-deposited (PLD) YBCO superconductor.

II. EXPERIMENTAL DETAILS

Details on the electrodeposition of $Gd_2Zr_2O_7$ and $Gd_2O_3/Gd_2Zr_2O_7$ are reported in a separate paper [5]. CeO_2 films were electrodeposited at 0.11 mA/ cm^2 under constant stirring from an electrodeposition bath containing 6 mM of cerium bromide dissolved in water. The average rate of deposition was about 5 nm/min.

Composition and thickness of electrodeposited films were obtained from inductively coupled plasma (ICP) analysis. Buffer films were characterized by X-ray diffraction (XRD) using copper Kα radiation (λ = 1.56054 Å). Phase identification was performed in Bragg Bretano geometry (θ/2θ geometry). The mosaic spread of $Gd_2Zr_2O_7$ and CeO_2 grains along the *c*-axis was obtained from omega scans on the (004) reflection [2θ=33.90 (±0.15)º] and (002) reflection [2θ= 33.24 (± 0.07)°], respectively. The angular dispersion of $Gd_2Zr_2O_7$ and CeO_2 grains in (*a*,*b*) plane was obtained from the peak broadening of phi scans on the (222) reflection [2θ=29.30 (±0.03)º and χ=54.7º] and (111) reflections [2θ= 28.55 (±0.03)º and χ=54.7º], respectively. Scanning electron microscopy (SEM) scans and optical profiler scans were used for morphology and film-roughness measurements.

The PLD system used to prepare the YBCO superconductor consisted of a standard PLD chamber (Neocera) and an excimer KrF laser (Lambda Physik, Compex 201, λ = 248 nm) operated at 260 mJ. The laser beam is focused onto a 3 x 1 mm^2 spot on a target at a 45° angle, with a fluence of 2–3 J/cm^2. The surface of the YBCO target was cleaned in situ by exposure to 1000 laser shots at 10 Hz prior to every deposition. The target-to-substrate distance was kept at 6 cm. Transport current densities in the YBCO layers were obtained from a four-probe measurement using the field criterion of 1 μV/cm.

Manuscript received 19 August 2008.

This work has been performed by an employee of the Midwest Research Institute under Contract No. DE-AC36-99GO10337 with the U.S. Department of Energy. The United States Government retains a non-exclusive, paid-up, irrevocable, worldwide license to publish or reproduce the published form of this work.

R.N. Bhattacharya, S. Phok, W. Zhao, and A. Norman are with the National Renewable Energy Laboratory, Golden, CO 80401 USA (phone: 303-384-6477; fax: 303-384-6432; e-mail: Raghu_bhattacharya@nrel.gov).

III. Results and Discussion

A. Growth conditions of ED-CeO_2/$Gd_2Zr_2O_7$ layers

Figure 1 shows the XRD patterns of several annealed 20-nm-thick CeO_2 on 60-nm-thick $Gd_2Zr_2O_7$ buffer layers. The annealing temperatures for this set of samples were in the range of 800 to 1100 °C. The XRD peaks identified as $Gd_2Zr_2O_7$ (004) reflection at $2\theta = 33.9$ (± 0.15)° and Ni-W (002) reflection at $2\theta = 51.6$ (± 0.03)° are the only ones observed. Although we did not observe any significant improvement in crystallinity and grain growth of $CeO_2/Gd_2Zr_2O_7$ buffers by increasing the annealing temperature from 800 to 1100 °C, high annealing temperature (>1000 °C) prevented the formation of misorientated peaks in the $Gd_2Zr_2O_7$ layer. The shoulder peak in the $Gd_2Zr_2O_7$ (004) indicates the presence of a ceria phase. Also, the large dispersion of ± 0.15° for $Gd_2Zr_2O_7$ 2θ positions indicates cerium-doped $Gd_2Zr_2O_7$ phases. The shift in the (004) peak position is caused by the doping of cerium atoms in the crystal structure of $Gd_2Zr_2O_7$. To obtain high-quality biaxially textured $CeO_2/Gd_2Zr_2O_7$ buffer layers, we found that the optimized annealing conditions were 1100 °C for 5 h.

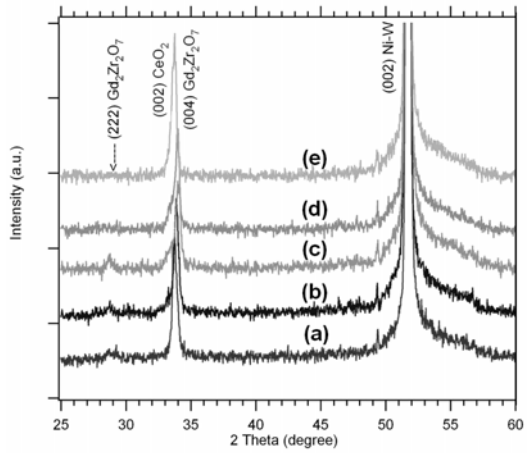

Fig. 1. X-ray diffraction of electrodeposited $CeO_2/Gd_2Zr_2O_7$ on Ni-W substrate after annealing in H_2:Ar gas flow at (a) 800, (b) 950, (c) 1000, (d) 1050, and (e) 1100 °C for 5 h.

B. Optimization of ED-CeO_2 cap layer thickness on ED-$Gd_2Zr_2O_7$/Ni-W

Ceria cap layers ranging in thickness from 10 to 80 nm were electrodeposited on ED-$Gd_2Zr_2O_7$/Ni-W. The thickness of the ceria layer was determined by ICP analysis. Figure 2 shows the XRD patterns of annealed $CeO_2/Gd_2Zr_2O_7$ buffer layers with CeO_2 thicknesses of (a) 10, (b) 20, (c) 40, (d) 60, and (e) 80 nm. In all these bilayers, the $Gd_2Zr_2O_7$ layer was 65 nm thick. The CeO_2 (002) reflection at $2\theta = 33.24$ (± 0.07)° was more prominent when the CeO_2 layer was thicker than 20 nm. As shown in Fig. 2, misorientation along the CeO_2 <111> axis is apparent when the thickness of the CeO_2 layer exceeds 40 nm.

Surface morphology of 60- and 80-nm-thick ED-CeO_2 cap layers on ED-$Gd_2Zr_2O_7$/Ni-W is shown in Fig. 3. Micrograph 3(a), representing 60-nm-thick CeO_2, shows smooth and crack-free surface morphology with a roughness of about 5 nm. The morphology of 10-, 20-, and 40-nm-thick ED-CeO_2 (not shown here) was also smooth and crack free, but when the thickness of ED-CeO_2 exceeded 60 nm, the surface roughness increased significantly and the film started to crack. Micrograph 3(b), of 80-nm-thick ED-CeO_2, shows a film roughness of about 11 nm and formation of cracks. Our previous work also suggests that doped or undoped CeO_2 with a thickness >80 nm tends to form cracks [7].

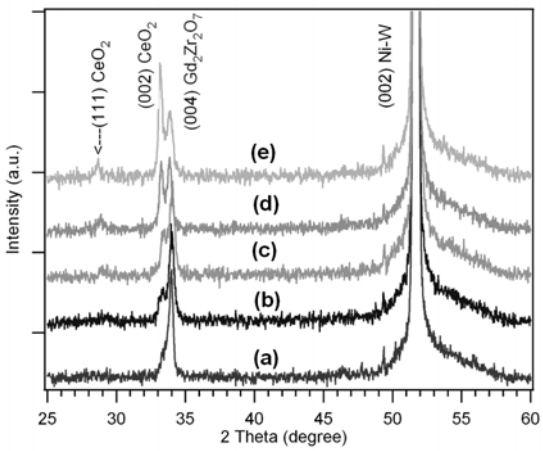

Fig. 2. X-ray diffraction of electrodeposited $CeO_2/Gd_2Zr_2O_7$ on Ni-W substrate with various thicknesses of CeO_2 layer: (a) 10, (b) 20, (c) 40, (d) 60, and (e) 80 nm after annealing in H_2:Ar gas flow at 1100 °C for 5 h.

The omega scan (out-of-plane alignment) of $Gd_2Zr_2O_7$ and CeO_2 for ED-CeO_2/ED-$Gd_2Zr_2O_7$/Ni-W structures is shown in Fig. 4. The omega scans of a 60-nm-thick ED-CeO_2/65-nm-thick ED-$Gd_2Zr_2O_7$/Ni-W layer structure showed a grain mosaic spread of 8.2° for ED-$Gd_2Zr_2O_7$ (Fig. 4a) and 7.5° for ED-CeO_2 (Fig. 4b). The omega scans of 20-nm-thick ED-CeO_2/65-nm-thick ED-$Gd_2Zr_2O_7$/Ni-W layer structures showed a grain mosaic spread of 6.9° (Fig. 4c) for the ED-$Gd_2Zr_2O_7$ layer. We could not measure the omega scan of the 20-nm ED-CeO_2 layer because it is very thin and the reflection position is very close to $Gd_2Zr_2O_7$ (004).

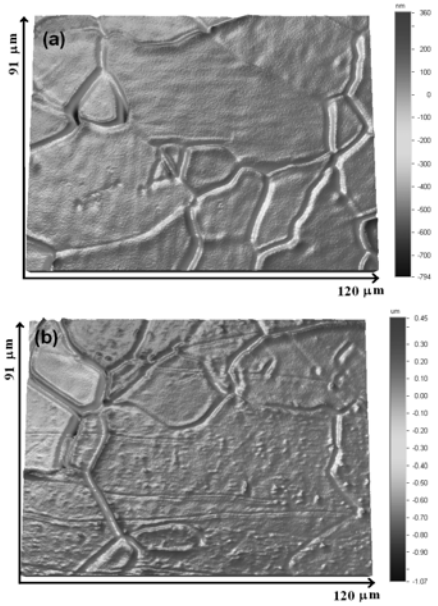

Fig. 3. Optical scans of annealed $CeO_2/Gd_2Zr_2O_7$ on Ni-W substrate with (a) 60-nm-thick CeO_2 and (b) 80-nm-thick CeO_2 cap layers.

The in-plane texture of $Gd_2Zr_2O_7$ and CeO_2 for ED-CeO_2/ED-$Gd_2Zr_2O_7$/Ni-W structures is shown in Fig. 5. Phi scans were performed on $Gd_2Zr_2O_7$ (222) and CeO_2 (111) reflections. The phi scans of 60-nm-thick ED-CeO_2/65-nm-thick ED-$Gd_2Zr_2O_7$/Ni-W layer structures showed a grain dispersion of 8.8° for ED-$Gd_2Zr_2O_7$ (Fig. 5a) and 9° for ED-CeO_2 layer (Fig. 5b). The phi scans of 20-nm-thick ED-CeO_2/65-nm-thick ED-$Gd_2Zr_2O_7$/Ni-W layer structures showed a grain dispersion of 7.8° (Fig. 5c) for the ED-$Gd_2Zr_2O_7$ layer. Here, also, we could not measure the phi scan of the 20-nm ED-CeO_2 layer because it is very thin and the reflection position is very close to $Gd_2Zr_2O_7$ (222).

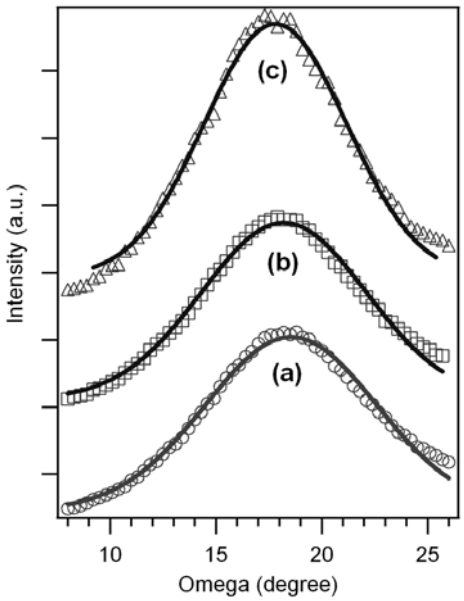

Fig. 4. Out-of-plane alignment of (a) a 65-nm $Gd_2Zr_2O_7$ (004) reflection at 2θ = 33.90°, (b) 60-nm CeO_2 (002) reflection at 2θ = 32.24° for the 60-nm CeO_2 on 65-nm $Gd_2Zr_2O_7$ bilayer structure, and (c) $Gd_2Zr_2O_7$ (004) reflection at 2θ = 33.90° for the 20-nm CeO_2 on 65-nm $Gd_2Zr_2O_7$ bilayer structure.

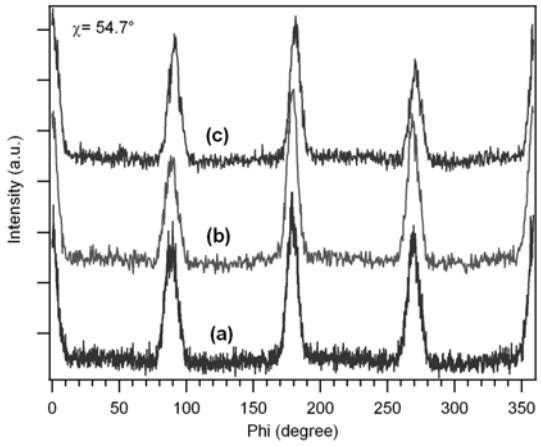

Fig. 5. In-plane alignment of (a) a 65-nm $Gd_2Zr_2O_7$ (222) reflection at 2θ =29.30°, (b) 60-nm CeO_2 (111) reflection at 2θ =28.55° for the 60-nm CeO_2 on 65-nm $Gd_2Zr_2O_7$ bilayer structure, and (c) $Gd_2Zr_2O_7$ (222) reflection at 2θ = 29.30° for the 20-nm CeO_2 on 65-nm $Gd_2Zr_2O_7$ bilayer structure.

The detailed microstructure of a 20-nm-thick CeO_2 on 65-nm-thick $Gd_2Zr_2O_7$ bilayer was analyzed by transmission electron microscopy (TEM) and energy dispersive x-ray spectrometry (EDS). Micrograph (a), which is a bright-field image of the full bilayer structure, revealed a nanoporous $Gd_2Zr_2O_7$ layer and a dense cap layer of CeO_2. The $Gd_2Zr_2O_7$ layer had a microstructure and pore density of about 10^{16} cm^{-3}, similar to Gd_2O_3/$Gd_2Zr_2O_7$ buffer architecture [6]. The cap layer CeO_2 does not have any voids (pores). The EDS line scan (Fig. 6b) indicates that interdiffusion of Ce, Gd, and Zr occurs. The XRD scan (Fig. 1), from which we concluded that the shift in the (004) peak position is caused by the doping of cerium atoms in the crystal structure of $Gd_2Zr_2O_7$, agrees with this EDS analysis result. The high-resolution TEM in Fig. 7 shows crystalline CeO_2 and $Gd_2Zr_2O_7$ layers without any defects.

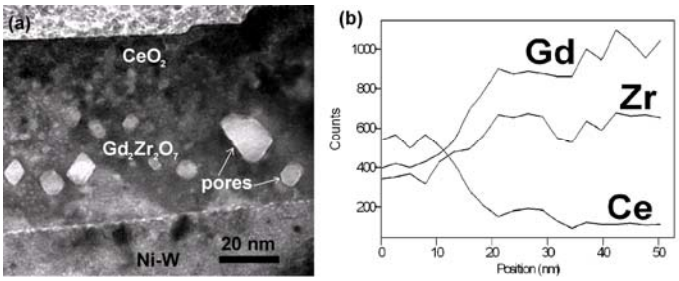

Fig. 6. TEM of CeO_2/$Gd_2Zr_2O_7$ on Ni-W substrate: (a) bright-field image and (b) EDS analysis of the CeO_2-$Gd_2Zr_2O_7$ interface.

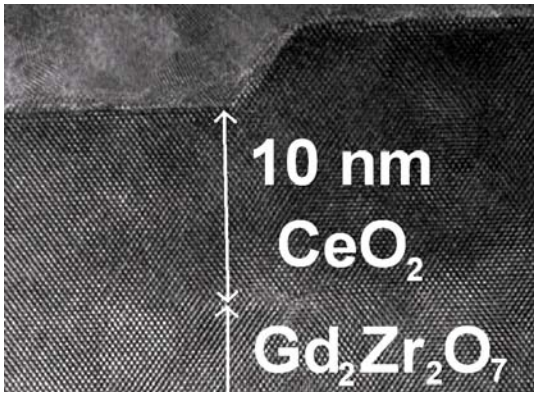

Fig. 7. HRTEM of the CeO_2-$Gd_2Zr_2O_7$ interface for ED-CeO_2/ ED-$Gd_2Zr_2O_7$ on Ni-W substrate.

C. YBCO pulsed laser deposition on electrodeposited Gd_2O_3/ $Gd_2Zr_2O_7$ and CeO_2/ $Gd_2Zr_2O_7$ bilayers

YBCO was deposited on Gd_2O_3/$Gd_2Zr_2O_7$ and CeO_2/$Gd_2Zr_2O_7$ to qualify the electrodeposited buffer layers. The deposition was carried out in 600 and 650 mTorr of oxygen and at temperatures varying from 720 to 780 °C for about 30 min with a pulse rate of 5 Hz. After deposition, the oxygenation treatment was performed at 500 °C for 30 min in 1 bar oxygen. The PLD-YBCO layer (300 nm thick) on Gd_2O_3/$Gd_2Zr_2O_7$ was biaxially textured as we have reported previously [8]. Table 1 summarizes the PLD conditions we have investigated and the resulting transport current density that was carried by the YBCO superconducting layer. Current densities greater than 1 MA/cm^2 were obtained for YBCO deposited at temperatures from 720 to 770 °C. In 600 mTorr oxygen, the optimal deposition temperature was 720 °C. A degradation of the superconducting current was observed

for YBCO deposited at 780 °C at 600 mTorr oxygen. At higher oxygen pressure (650 mTorr), the optimal temperature was found to be 755 °C. The YBCO layer with a current of 3.3 MA/cm^2 was prepared at 755°C in 650 mTorr oxygen.

TABLE I. PLD YBCO ON SIMPLIFIED ELECTRODEPOSITED BUFFERS

Buffer architecture	Partial oxygen pressure (mTorr)	Temperature (°C)	Transport current density (MA/cm^2)
Gd_2O_3/ $Gd_2Zr_2O_7$	600	720	2
	600	730	1
	600	740	1.2
	600	750	1.4
	600	760	1.2
	600	770	1
	600	780	0.2
	650	745	1.7
	650	755	3.3
CeO_2/ $Gd_2Zr_2O_7$	650	745	0.5
	650	755	0.1

Pulsed laser deposition conditions of YBCO on Gd_2O_3/$Gd_2Zr_2O_7$ and CeO_2/$Gd_2Zr_2O_7$, and current measurements of the superconducting layer.

The morphology and microstructure of PLD YBCO deposited on an ED-Gd_2O_3/$Gd_2Zr_2O_7$ buffer architecture at 720 °C and 600 mTorr are shown in Fig. 8. Figure 8a shows the SEM surface view of YBCO. The SEM micrograph indicates the liquid-phase formation during the YBCO growth with void sizes of 500 nm. Micrograph (b) is a high-resolution TEM image showing the interface and crystal orientation of YBCO and the Gd_2O_3 cap layer. A clean interface was observed between the superconductor and the buffer layer. No impurity phases or misorientations were detected in the YBCO and Gd_2O_3 layers. An epitaxial relationship of YBCO {001} planes parallel to Gd_2O_3 {001} planes is clearly seen.

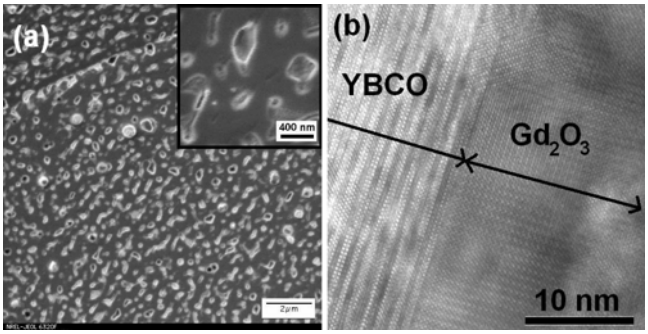

Fig. 8. Typical morphology and microstructure of PLD YBCO deposited at 720 °C in p(O_2)= 600 mTorr on Gd_2O_3/$Gd_2Zr_2O_7$ buffer layers: (a) SEM image of a surface view and (b) HRTEM of YBCO-Gd_2O_3 interface.

We also investigated the deposition of PLD-YBCO on a 20-nm CeO_2/$Gd_2Zr_2O_7$ layer. PLD deposition was performed at 650 mTorr oxygen. Resulting YBCO current densities are presented in Table 1. Transport current measurement revealed low current densities in the range of 0.1–0.5 MA/cm^2. At present, we are optimizing the ED-CeO_2/$Gd_2Zr_2O_7$ bilayers to obtain high-current-carrying YBCO superconductor.

IV. CONCLUSION

High-performance PLD YBCO films have been demonstrated on electrodeposited Gd_2O_3/$Gd_2Zr_2O_7$ buffer architecture. A high density (~10^{16} cm^{-3}) of nanometer-scale voids was observed in the $Gd_2Zr_2O_7$ layer, but no voids were present in the Gd_2O_3 and CeO_2 layers. The electrodeposition process is a potentially low-cost, scalable processing technology and deserves more attention.

ACKNOWLEDGMENT

We thank Bobby To of the National Renewable Energy Laboratory for SEM analysis. We are also grateful to M. Paranthaman of Oak Ridge National Laboratory for providing Ni-W tapes.

REFERENCES

[1] A. Goyal, D.P. Norton, D.K. Christen, E.D. Specht, M. Paranthaman, D.M. Kroeger, J.D. Budai, Q. He, F.A. List, R. Feenstra, H.R. Kerchner, D.F. Lee, E. Hatfield, P.M. Martin, J. Mathis, and C. Park, "Epitaxial superconductors on rolling-assisted biaxially-textured substrates (RABiTS): A route towards high critical current density wire", *Applied Superconductivity*, vol. 4, pp. 403-427, 1996.

[2] T. Aytug; M. Paranthaman, S. Sathyamurthy, B.W. Kang, D.B. Beach, C.E. Vallet, E.D. Specht, D.F. Lee, R. Feenstra, A. Goyal, D.M. Kroeger, K.J. Leonard, P.M. Martin, and D.K. Christen, "High-Jc YBCO coatings on reel-to-reel dip-coated Gd_2O_3 seed buffer layers epitaxially fabricated on biaxially textured Ni and Ni-(3at%W-1.7at%Fe) alloy tapes", *Mater Res Soc Symp Proc,* vol. 689, pp.211-216, 2002.

[3] X.D. Wu, R.C. Dye, R.E. Muenchausen, S.R. Foltyn, M. Maley, A.D. Rollett, A.R. Garcia, and N.S. Nogar, "Epitaxial CeO_2 Films as Buffer Layers for High-Temperature Superconducting Thin-Films", *Appl. Phys. Lett.,* vol. 58, pp. 2165-2167, 1991.

[4] R. Bhattacharya, S. Phok, P. Spagnol, and T. Chaudhuri, "Electrodeposited Biaxially Textured Buffer Layer for $YBa_2Cu_3O_{7-\delta}$ (YBCO) Superconductor Oxide Film", *J. Electrochem. Soc.*, vol. 153, pp. C273-C276, 2006.

[5] S. Phok, W. Zhao, and R. Bhattacharya, "Growth Conditions of Sequentially Electrodeposited Layers for YBCO Superconductors", *IEEE Trans. Appl. Supercond.*, submitted for publication.

[6] W. Zhao, A. Norman, S. Phok, and R. Bhattacharya, "Transmission electron microscope study on electrodeposited Gd_2O_3 and $Gd_2Zr_2O_7$ buffer layers for $YBa_2Cu_3O_{7-d}$ superconductors", *Physica C*, vol. 468, pp. 1092-1096, 2008.

[7] S. Phok and R. Bhattacharya, "Effect of samarium doping on electrodeposited CeO_2 thin film", *Phys. Stat. Sol. (a)*, vol. 203, no. 15, pp. 3734-3742, 2006.

[8] R. Bhattacharya and S. Phok, "Electrodeposited $Gd_2Zr_2O_7$ and Gd_2O_3 Buffer Layers for $YBa_2Cu_3O_{7-\delta}$ Superconductors", *J. Electron. Mater.*, vol. 36 no. 10, pp. 1275-1278, 2007.